Published in final edited form as:

Clin Cancer Res. 2019 July 15; 25(14): 4332–4342. doi:10.1158/1078-0432.CCR-18-3312.

Specific targeting of somatostatin receptor subtype-2 for fluorescence-guided surgery

Servando Hernandez Vargas[1], **Susanne Kossatz**[2], **Julie Voss**[1], **Sukhen C. Ghosh**[1], **Hop S. Tran Cao**[3], **Jo Simien**[1], **Thomas Reiner**[2,4], **Sadhna Dhingra**[5], **William E. Fisher**[3], **Ali Azhdarinia**[1]

[1]The Brown Foundation Institute of Molecular Medicine, McGovern Medical School, The University of Texas Health Science Center at Houston, Texas 77030, USA.

[2]Department of Radiology, Memorial Sloan Kettering Cancer Center, New York, New York 10065, USA

[3]Michael E. DeBakey Department of Surgery, Baylor College of Medicine, Houston, Texas 77030, USA

[4]Department of Radiology, Weill Cornell Medical College, New York, New York 10065, USA

[5]Department of Pathology & Immunology, Baylor College of Medicine, Houston, Texas 77030, USA

Abstract

Purpose: Clinically available intraoperative imaging tools to assist surgeons in identifying occult lesions are limited and partially responsible for the high rate of disease recurrence in patients with neuroendocrine tumors (NETs). Using the established clinical efficacy of radiolabeled somatostatin analogs as a model, we demonstrate the ability of a fluorescent somatostatin analog to selectively target tumors that overexpress somatostatin receptor subtype-2 (SSTR2) and demonstrate utility for fluorescence-guided surgery (FGS).

Experimental design: A multimodality chelator (MMC) was used as a “radioactive linker” to synthesize the fluorescently labeled somatostatin analog, $^{67/68}$Ga-MMC(IR800)-TOC. *In vivo* studies were performed to determine the pharmacokinetic profile, optimal imaging time point, and specificity for SSTR2-expressing tissues. Meso- and microscopic imaging of resected tissues and frozen sections were also performed to further assess specific binding, and binding to human NETs was examined using surgical biospecimens from patients with pancreatic NETs.

Correspondence and requests for materials should be addressed to A.A. (ali.azhdarinia@uth.tmc.edu, tel: 713-500-3577, fax: 713-500-0319).

Author contributions

A.A. designed and supervised the project; S.H.V., J.V., and S.K. contributed to the study design. S.H.V. and S.G. performed the chemistry and radiochemistry experiments; S.H.V. and J.V. performed the *in vivo* imaging studies; S.H.V., S.K., J.S. and S.D. performed the histological studies. W.E.F. provided surgical biospecimens. S.H.V., S.K., J.V., and A.A. analyzed the data. S.H.V., S.K., and A.A. wrote the manuscript with valuable input from H.S.T.C. and T.R. All authors read and approved the manuscript.

The authors declare no potential conflicts of interest.

Supplementary data

Supporting Information for this article including supplementary Figures and Tables are available in the online version of the paper.

Results: Direct labeling with $^{67}Ga/^{68}Ga$ provided quantitative biodistribution analysis that was in agreement with fluorescence data. Receptor-mediated uptake was observed *in vivo* and *ex vivo* at the macro-, meso, and microscopic scales. Surgical biospecimens from patients with pancreatic NETs also displayed receptor-specific agent binding, allowing clear delineation of tumor boundaries that matched pathology findings.

Conclusions: The radioactive utility of the MMC allowed us to validate the binding properties of a novel FGS agent that could have a broad impact on cancer outcomes by equipping surgeons with real-time intraoperative imaging capabilities.

Keywords

fluorescence-guided surgery; cancer surgery; dual-labeling; near-infrared fluorescence imaging; somatostatin receptor

Introduction

Neuroendocrine tumors (NETs) are slow growing tumors that produce significant morbidity and eventual mortality. The diagnosis of NETs has increased nearly five-fold over the last three decades (1) and is predicted to continue rising at a faster rate than other common cancers such as breast and lung cancer (2). Similar to most cancers, surgery remains the only curative treatment option for patients with NETs. Unique to this patient population, however, is that surgery is indicated not only for localized lesions, but also for advanced tumors to control excessive hormone production by debulking the metastatic disease burden (3). Thus, surgery can improve overall survival in both NET patients with localized disease and those with metastatic disease who comprise more than 50% of clinical cases. While surgery can be curative if all cancer cells are removed, patients with NETs have a 5-year recurrence rate of 94% (4). Improved identification and resection of these lesions would have a major impact on surgical efficacy and outcomes for NET patients.

In recent years, intraoperative tools that enable real-time tumor visualization have emerged. One approach, known as fluorescence-guided surgery (FGS), can help surgeons identify tumor margins with higher accuracy, which is crucial for achieving complete tumor resection and minimizing local recurrence (5). This may also reduce the need for additional surgeries and can limit removal of healthy tissues. In NETs, intraoperative imaging could also increase tumor detection rates, enhance primary tumor localization for enucleation, and identify small lesions and locoregional disease with lymph node involvement to improve surgical outcomes. Despite the growing number of fluorescent contrast agents entering clinical trials, validated intraoperative imaging agents are currently lacking for this patient population. Conversely, radiolabeled somatostatin analogs have a long history of use in nuclear medicine and positron emission tomography (PET), and are considered to be the gold standard for noninvasive imaging of NETs (6–11). Moreover, radiolabeled somatostatin analogs are currently used pre-operatively for surgical planning and post-operatively for surveillance. In order to extend the utility of PET into the operating room, our group developed the first bioactive fluorescent analog of a clinical radiotracer using 1,4,7,10-tetraazacyclododecane-1,4,7,10-tetraacetic acid-Tyr^3-octreotide (^{68}Ga-DOTA-TOC) as a model (12). We introduced a synthesis scheme that enabled conversion of ^{68}Ga-DOTA-TOC

into a dual-labeled counterpart, ^{68}Ga-MMC(IR800)-TOC, where MMC represents a multimodality chelator that replaces the standard chelating agent, DOTA (Fig. 1). *In vitro* studies demonstrated excellent retention of somatostatin receptor subtype-2 (SSTR2) binding and specificity after dye conjugation, and biodistribution in healthy mice identified the kidneys as the major excretion organ.

In the present study, we examine the tumor targeting properties of Ga-MMC(IR800)-TOC in SSTR2-expressing xenografts to determine effectiveness for FGS. Near-infrared fluorescence (NIRF) imaging was performed to determine the imaging time point that produces optimal tumor contrast, and radiolabeled analogs were prepared to quantitatively measure tracer biodistribution. Tumor specificity was examined by *in vivo* NIRF imaging, followed by *ex vivo* NIRF imaging of tissues and frozen sections. To determine the translational utility of Ga-MMC(IR800)-TOC, binding was evaluated in surgical biospecimens from patients with pancreatic NETs. Specificity for tumor tissue and SSTR2 were determined by histology and confocal microscopy, respectively.

Materials and Methods

General methods

All chemicals were purchased from Sigma-Aldrich unless otherwise noted. Reversed-phase high-performance liquid chromatography (HPLC) was performed on an analytical Hitachi LaChrom system using a Kinetex C18 column (2.6 μm) (Phenomenex) with a mobile phase of A = 0.1% TFA in H_2O, B = 0.1% TFA in CH_3CN (gradient: 0 min, 10% B; 12 min, 90% B); flow rate, 1 mL/min. Radiochemical purities of ≥95% were assessed by radio-high-performance liquid chromatography (radio-HPLC) using an in-line radioactive detector (Berthold Technologies). Electrospray ionization (ESI) mass spectra were acquired on a LCQ FLEET instrument (Thermo Scientific).

Labeling of MMC(IR800)-TOC with ^{68}Ga, ^{67}Ga, and Ga

Radiolabeling was performed using a cation exchange cartridge as previously described (12). Following Sep-Pak Light C18 (Waters) purification, the product was diluted with PBS and analyzed by radio-HPLC. ^{67}Ga-citrate was purchased from a radiopharmacy (Cardinal Health) and was added to an equal volume of 0.1 M HCl to produce $^{67}GaCl_3$. The radioactive solution was then processed identically to generator-produced ^{68}Ga with the exception of using 0.5 M ammonium acetate (pH 4.5) as the reaction buffer. Cold Ga labeling was performed according to methods established above for the radiolabeled compounds. MMC(IR800)-TOC (60 nmol) was mixed with a 4-fold molar excess of $GaCl_3$ and heated at 95°C for 15 min. The crude mixture was purified by ultrafiltration and the pure product was characterized by HPLC and mass spectrometry.

Cell culture and animal models

Athymic female nu/nu mice (Charles River Laboratories) were housed under standards of the Institutional Animal Care and Use Committee (IACUC) of the University of Texas Health Science Center at Houston and maintained on normal rodent chow. HCT116-SSTR2 (courtesy of Dr. Buck Rogers, Washington University in St. Louis, and Dr. Carolyn J.

Anderson, University of Pittsburgh), HCT116-WT (ATCC), and NCI-H69 (ATCC) cell lines were cultured in Roswell Park Memorial Institute (RPMI) 1640 medium with 10% (v/v) Fetal Bovine Serum (FBS) and maintained at 37°C with 95% humidity and 5% CO_2 atmosphere. HCT116-SSTR2 cells were additionally supplemented with 100 μg/ml Zeocin (Gibco). For all procedures, mice were anesthetized with 1–2% isoflurane. For xenografting, 6–8 week old mice were subcutaneously injected with 1×10^6 HCT116-SSTR2, 1×10^6 HCT116-WT, or 5×10^6 NCI-H69 cells in matrigel (Corning):PBS (1:1) in the shoulder. Studies were conducted 3–4 weeks post implantation when tumor size reached approximately 5–10 mm maximum diameter. Overdose of anesthesia followed by cervical dislocation was the method of euthanasia for mice in terminal studies.

In vitro studies

Radioactive uptake studies were performed as previously described (12). Briefly, HCT116-SSTR2, NCI-H69 and non-SSTR2 expressing HCT116-WT cells (200,000 cells/well) were incubated with a 10 nM solution of ^{68}Ga-MMC(IR800)-TOC, ^{68}Ga-DOTA-TOC or a mixture of radiotracer with a 100-fold excess of octreotide at 37°C for 1 h. After incubation and washing, cells were collected and radioactivity was quantified in a Wizard^2 automated γ counter (Perkin Elmer) to determine uptake as percent of total radioactivity added.

Fluorescence imaging of Ga-MMC(IR800)-TOC cellular uptake was performed as previously described (12). Briefly, HCT116-SSTR2 and HCT116-WT cells were plated (50,000 cells/well), allowed to attach for 48 hours and incubated with 5 μM Ga-MMC(IR800)-TOC for 1 hour at 37°C. NCI-H69 cells were identically processed with the exception of being in suspension. After the incubation period cells were washed with media two times for 5 min. Subsequently, cells were fixed. NCI-H69 cells were immobilized onto Shi-fix coverslips (Everest Biotech, Oxfordshire, UK) following the manufacturers' instructions. Cells were mounted with Mowiol mounting medium containing Nucspot Live 488 nuclear stain (diluted 1:1000 in Mowiol) and microscopic images were acquired on a confocal microscope (SP8, Leica). IR800 was detected using a 730 nm laser and NucSpot Live 488 was detected using a 488 nm laser with appropriate filter settings.

In vivo stability of ^{67}Ga-MMC(IR800)-TOC

Athymic female nu/nu mice were intravenously injected with 15 nmol (42.5 μg) of ^{67}Ga-MMC(IR800)-TOC. Blood samples were obtained by post-mortem exsanguination of the heart 24 h post-injection and centrifuged to isolate the plasma. Ice cold acetonitrile was then added to an equal volume of the plasma to precipitate plasma proteins. Finally, the supernatant was collected and analyzed by HPLC based on emission in the fluorescent channel with conditions as stated in the General Methods section.

In vivo imaging

Mice with HCT116-SSTR2 tumors (n = 5) were intravenously injected with Ga-MMC(IR800)-TOC (2 nmol, 5.67 μg) and imaging was performed at 3 and 24 h post-injection. *In vivo* NIRF images were acquired for 200 ms without background subtraction using a custom-built electron-multiplying charge-coupled device (EMCCD) fluorescence imaging system at $\lambda_{ex}/\lambda_{em}$ = 785/830 nm (13), and image analysis was performed with the

ImageJ software package (NIH). At the conclusion of the imaging studies, the mice were euthanized and selected organs were excised and underwent *ex vivo* NIRF imaging using an IVIS Lumina II (Perkin Elmer). To demonstrate feasibility of imaging with a clinically approved system, mice bearing HCT116-SSTR2 tumors were intravenously injected with Ga-MMC(IR800)-TOC (5 nmol, 14.2 μg) and imaged using the Firefly fluorescence imaging system on the da Vinci surgical robot (λ_{ex} = 805 nm; Intuitive). NIRF images were acquired under ambient room lighting at 3 and 48 h post-injection.

Ex vivo imaging and biodistribution

Mice with HCT116-SSTR2 tumors were intravenously injected with 370 kBq (10 μCi, 2 nmol) of ^{68}Ga-MMC(IR800)-TOC or ^{67}Ga-MMC(IR800)-TOC and euthanized at 3, 24, or 48 h post-injection. Selected tissues were excised and underwent *ex vivo* optical imaging on the IVIS with the following settings: lamp level (high), excitation (745 nm), emission (ICG), epi-illumination; binning (S); FOV (C, 10); f-stop (2); acquisition time (1 s). Region-of-interest (ROI) analysis was performed with the vendor software package (Living Image) to obtain tumor-to-background ratios (TBR). Parameters were the same for all acquired images. At the completion of the optical imaging studies, tissues were weighed and counted for radioactivity using the γ counter. The total injected activity per mouse was determined from an aliquot of the injected solutions. The results are expressed as a percentage of the injected activity per gram of tissue (%IA/g) and represent the mean ± SD of n = 5 mice/time point. To demonstrate SSTR2-binding in an animal model with endogenous receptor expression, xenografts were prepared using NCI-H69 human small cell lung cancer cells and biodistribution was performed at 48 h post-injection.

In vivo specificity and multiscale localization of tracer uptake

For specificity studies, Ga-MMC(IR800)-TOC (2 nmol) uptake in HCT116-SSTR2 was compared to SSTR2-negative HCT116-WT xenografts by *in vivo* and *ex vivo* optical imaging at 24 h post-injection. Tumors and key organs (muscle, pancreas, small intestine) were cryoconserved in OCT and used to prepare frozen sections (10 μm) for mesoscopic and microscopic analysis to localize the IR800 signal within the tissue. Using an Odyssey slide scanner (LiCOR), sections were scanned and fluorescence intensities at 800 nm were quantified on 16-bit images using ImageJ. ROIs were drawn around the outline of each organ and means ± SD were calculated using GraphPad Prism (n=3 mice/group). Adjacent sections underwent hematoxylin and eosin (H&E) staining to permit morphological analysis of the tissue.

To analyze Ga-MMC(IR800)-TOC distribution and receptor specificity at the cellular level, the frozen sections were fixed in 4% cold paraformaldehyde for 10 min and embedded in Mowiol mounting medium. For counterstaining, we added NucSpot Live 488 nuclear stain (Biotium) to the mounting medium (1:1000 dilution directly in Mowiol) and NIRF confocal microscopy was performed.

Ex vivo staining of human NET biospecimens with Ga-MMC(IR800)-TOC

In order to evaluate the binding and specificity of Ga-MMC(IR800)-TOC in human tumor tissues that express SSTR2, surgical biospecimens of pancreatic NETs and surrounding

normal tissue were obtained from the Elkins Pancreas Center at Baylor College of Medicine. The use of tissues was approved by the Institutional Review Boards of Baylor College of Medicine and The University of Texas Health Science Center. All patients gave written informed consent. Biospecimens (n=5) were fresh frozen and used to prepare 4 μm frozen sections for *ex vivo* staining with Ga-MMC(IR800)-TOC. Frozen sections were thawed at room temperature for 15 min and briefly wetted with PBS. A 5 μM solution of Ga-MMC(IR800)-TOC was added onto the slide and incubated for 45 min at 37 ºC. Slides were then washed twice for 3 min with PBS. Fixation was performed in 4% cold paraformaldehyde for 10 min and slides were mounted with Mowiol mounting medium containing Nucspot Live 488 nuclear stain (diluted 1:1000 in Mowiol). Subsequently, NIRF confocal microscopy was performed. Sections stained with H&E were used for correlation of tissue morphology.

Immunofluorescence staining of SSTR2

To detect SSTR2 expression, IHC was carried out on frozen sections of xenograft tumor tissue (HCT116-SSTR2, HCT116-WT) and human NET biospecimens using the Discovery XT processor (Ventana Medical Systems, Tucson, AZ) at the Molecular Cytology Core Facility of Memorial Sloan Kettering Cancer Center. After thawing, sections were baked at 50ºC for 1 h, followed by a 30 min incubation with Background Buster solution (Innovex, Richmond, CA). Sections were then incubated with the anti-SSTR2 rabbit monoclonal antibody (Abcam) at 2.2 μg/ml for 5 h, followed by a 1 h incubation with biotinylated goat anti-rabbit IgG (Vector Labs). For detection, a DAB detection kit (Ventana Medical Systems) was used according to the manufacturer instructions. Sections were counterstained with H&E and cover-slipped with Permount (Fisher Scientific). Slides were digitalized using a MIRAX Slide Scanner (3DHISTECH).

Statistical analysis

Curve fitting and linear regression calculations were performed with GraphPad Prism (v 5.01). All data are presented as mean ± standard deviation (SD) and group comparisons were performed with two-tailed t-tests.

Results

Radiochemistry and stability

Supplementary Fig. 1 shows a representative HPLC trace for ^{68}Ga-MMC(IR800)-TOC and ^{67}Ga-MMC(IR800)-TOC. Radiochemical yields were 78.2±8.1% and 72.7±4.1% for ^{68}Ga-MMC(IR800)-TOC and ^{67}Ga-MMC(IR800)-TOC, respectively, and purity of >99% was achieved after Sep-Pak purification. Serum stability studies showed >60% intact radiotracer at 24 h with minor metabolite formation (Supplementary Fig. 2).

In vivo imaging

Longitudinal NIRF imaging of Ga-MMC(IR800)-TOC was performed in HCT116-SSTR2 xenografts to determine the pharmacokinetic profile of the agent and subsequent effects on contrast at early (3 h) and delayed (24 h) time points. Ga-MMC(IR800)-TOC uptake was observed in the tumor region at 3 h but was also accompanied by notable background

fluorescence in the thoracic/abdominal regions and high kidney signal (Figs. 2a and Supplementary Fig. 3). At 24 h, a more focal pattern of agent uptake was evident in all tumors, along with lower background signal. ROI analysis revealed similar tumor fluorescence at 3 and 24 h ($5.6\pm0.9\times10^5$ and $4.2\pm1.4\times10^5$ counts/pixel^2, respectively, $P > 0.05$) but showed a 2-fold reduction in background fluorescence at 24 h ($4.8\pm1.0\times10^5$ to $2.3\pm1.0\times10^5$ counts/pixel^2, $P < 0.005$) (Fig. 2b), thus identifying clearance from normal tissues as the primary reason for improved tumor visualization with delayed imaging. These findings were in agreement with images acquired from the Firefly system (Supplementary Fig. 4).

Quantitative *ex vivo* analysis and contrast determination

MMC(IR800)-TOC was radiolabeled with ^{68}Ga or ^{67}Ga and injected into HCT116-SSTR2 xenografts for early (3 h) and delayed (24 and 48 h) analysis of agent uptake, respectively, by NIRF imaging and gamma counting. Macroscopic evaluation by *ex vivo* IVIS imaging revealed similar tumor fluorescence at 3, 24, and 48 h, along with high uptake in the kidneys and moderate uptake in the liver (Fig. 3a). Notable fluorescence was also seen in the lungs at 3 h, but was progressively reduced to background levels at 48 h. Signal in other tissues was minimal. Image analysis was performed to obtain semi-quantitative measurements of fluorescence intensity (Fig. 3b and Supplementary Table 1). Tumor signal was higher than all non-clearance organs and showed no significant differences between early and delayed time points. Clearance was primarily through the kidneys, which showed high fluorescence throughout. Conversely, fluorescence in all other tissues decreased as a function of time. From 3 to 48 h, the highest percentage of signal washout in normal tissues occurred in the muscle (77.0%, $P < 0.001$), small intestine (81.5%, $P < 0.001$) and lungs (86.8%, $P < 0.001$). This, in turn, lead to a 3.4, 4.1, and a 5.4-fold increase in tumor-to-muscle, tumor-to-small intestine and tumor-to-lung ratios, respectively ($P < 0.01$) (Fig. 3c). Importantly, ratios in key sites of NET formation with endogenous SSTR2 expression (pancreas, small intestine, and lungs) (14) ranged from 4.3–17.2, which is critical since a TBR of at least 2 is generally suitable for tumor delineation in the operating room.

Radioactive biodistribution results are summarized in Fig. 3d and Supplementary Table 2. At 3 h, administration of ^{68}Ga-MMC(IR800)-TOC resulted in high renal clearance (45.6±3.8 %IA/g), along with prominent accumulation in the lungs (6.7±0.9 %IA/g), liver (5.0±0.9 %IA/g), and stomach (4.5±0.8 %IA/g). Tumor uptake was notable (3.54±0.85 %IA/g) and higher than pancreas (1.7±0.2 %IA/g) and small intestine (1.3±0.1 %IA/g). At 24 and 48 h, ^{67}Ga-MMC(IR800)-TOC biodistribution showed excellent agent retention in tumors with %IA/g values of 4.3±1.1 and 6.7±0.9, respectively, whereas nearly all non-clearance organs had significantly lower uptake. At 48 h, signal had decreased by 61.2% in muscle ($P < 0.01$) and 95.9% in blood ($P < 0.001$), giving tumor-to-muscle and tumor-to-blood ratios of 34.2±14.0 and 81.0±35.3, respectively, which translated into a 5.7-fold (muscle) and 50.3-fold (blood) increase from values obtained at 3 h (Fig. 3e). Notably, TBRs improved for the lungs, pancreas, and small intestine to final values of 4.5±0.6 (8.6-fold increase), 5.8±1.3 (2.7-fold increase), and 8.2±1.1 (2.9-fold increase), respectively ($P < 0.001$).

A major limitation in NET research is the lack of robust orthotopic or patient-derived xenograft (PDX) animal models that accurately represent human disease. For further agent evaluation, we selected NCI-H69 cells, which are known to endogenously express moderate to low levels of SSTR2 (15) and have been widely used for assessment of SSTR2-targeted agents (16–20). As anticipated, *in vitro* results demonstrated specific binding and internalization in NCI-H69 cells (Supplementary Fig. 5 and Supplementary Fig. 6) at lower levels than HCT116-SSTR2 cells, but higher than non-SSTR2 expressing HCT116-WT cells. In line with these findings, we observed modest *in vivo* tumor uptake in NCI-H69 (1.2±0.4 %IA/g; Supplementary Fig. 7 and Supplementary Table 3) compared to HCT116-SSTR2 cells. Nevertheless, low background signal still produced optical contrast ratios that were >2 in the muscle, small intestine, and lung (Supplementary Fig. 7b).

Specificity for SSTR2 imaging *in vivo*

In order to demonstrate SSTR2-mediated targeting *in vivo*, Ga-MMC(IR800)-TOC uptake was compared in mice bearing HCT116-SSTR2 or HCT116-WT tumors. *In vivo*, high NIRF signal intensity was observed in SSTR2-overexpressing tumors while wild-type tumors were poorly delineated (Fig. 4a). Examination of resected tissue by *ex vivo* imaging (IVIS) confirmed *in vivo* results (Fig. 4b) and showed higher fluorescence in HCT116-SSTR2 tumors ($P < 0.01$) compared to the wild-type counterparts (Fig. 4c). This, in turn, resulted in TBRs that were 1.8, 1.8, 2.3, and 2.4-fold higher in the muscle, pancreas, small intestine, and lungs of HCT116-SSTR2 mice, respectively (Fig. 4d).

To enable evaluation of receptor specificity at the mesoscopic level, frozen sections of tumors that were injected with 2 nmol Ga-MMC(IR800)-TOC 24 h prior to necropsy were scanned on a slide scanner and showed localized Ga-MMC(IR800)-TOC uptake only in HCT116-SSTR2 tumors (Fig. 5a). Comparison to H&E staining revealed that uptake was confined to viable areas of the HCT116-SSTR2 tumors. Excellent co-localization was demonstrated between the Ga-MMC(IR800)-TOC signal and SSTR2 expression as determined by anti-SSTR2 IHC staining (Supplementary Fig. 8). Quantification of the Ga-MMC(IR800)-TOC signal showed, on average, 8.6-fold higher fluorescence signal in HCT116-SSTR2 tumors compared to HCT116-WT tumors, while signals in the pancreas, muscle, and small intestine were low and similar between the groups (Fig. 5b). Further validation of receptor specificity was shown by confocal microscopy, which revealed Ga-MMC(IR800)-TOC fluorescence in HCT116-SSTR2 tumors but not in HCT116-WT tumors (Fig. 5c). NIRF signal was observed at the cell membrane and intracellularly, in accordance with the SSTR2 staining, and indicates that Ga-MMC(IR800)-TOC was internalized with the receptor upon binding.

Ex vivo evaluation in human NET biospecimens

A proof-of-principle approach was used to show Ga-MMC(IR800)-TOC binding and specificity in human NETs. To simulate *in vivo* binding in patients, we developed an *ex vivo* staining protocol on fresh frozen sections of biospecimens (n=4) from pancreatic NET patients that consisted of tumor and surrounding non-tumor, pancreatic tissue for each patient. We first confirmed receptor expression *via* SSTR2 IHC, which clearly delineated tumor from normal tissue in accordance with H&E staining (Fig. 6a). The receptor was most

abundant at the cell membranes of tumor cells, while the staining was at background levels in non-tumor tissue. Staining of unfixed frozen sections with Ga-MMC(IR800)-TOC resulted in active binding to tumor tissue. This produced NIR fluorescence that was localized to the cell membrane and was very low in stromal areas and non-tumor tissue, in excellent agreement with SSTR2 IHC (Fig. 6b, Supplementary Fig. 9a). We were also able to confirm binding using a NIRF slide scanner, which showed that the emitted NIRF signal from Ga-MMC(IR800)-TOC was within the tumor boundaries identified by H&E staining and absent in normal tissues, indicating excellent specificity of the agent for human NETs and potential tumor delineation capability (Supplementary Fig. 9b).

Effect of injected dose on image contrast

Given the importance of achieving maximal fluorescent contrast for surgical applications, the relationship between injected dose and contrast was studied by comparing the effects of low (0.5 nmol) and high (2 nmol) dose administration of Ga-MMC(IR800)-TOC in SSTR2-expressing tumors at 24 h (Supplementary Fig. 10a). Although *ex vivo* imaging showed that absolute tumor fluorescence was 3.8-fold higher ($P < 0.001$) following injection of the higher dose (Supplementary Fig. 10b), fluorescence in non-tumor tissues was also elevated and, importantly, resulted in a >6-fold increase in background signal in the pancreas, small intestine, and lungs ($P < 0.001$). Since signal in background tissues was essentially absent with 0.5 nmol dose, the corresponding contrast ratios were higher for this group and increased by approximately 40% for each tissue compared to the high dose group (Supplementary Fig. 10c).

Discussion

Our findings show that a fluorescent somatostatin analog can be used to differentiate tumor from normal tissues based on highly specific targeting of SSTR2. Importantly, we also demonstrate that the MMC is an ideal linker since it produces a bioactive fluorescent analog of ^{68}Ga-DOTA-TOC and enables quantitative analysis. FGS agent design approaches from our group and others have benefited immensely from the successful first-in-human application of a targeted fluorescent agent by Van Dam *et al.* (21), which represented a major milestone in the field of FGS and played an important role in the development of new dyes and targeted probes (22), optimization of optical imaging systems, and identification of appropriate metrics and validation methods (23,24). Translational initiatives for FGS can be further complemented by combining the strengths of nuclear and optical imaging. Clinically, the addition of a radiolabel to a fluorescent agent has the potential to enhance the detection of deep-seated tumors by adding intraoperative gamma probe guidance to existing surgical imaging tools, such as intraoperative ultrasound (25,26). However, radiolabeling may be even more significant in the preclinical setting, where quantitative validation is critical for developing an expansive translational pipeline of targeted fluorescent contrast agents (27,28). Instead of applying our strategy to a novel targeting agent or biomarker, we exploited the established clinical effectiveness of radiolabeled somatostatin analogs to develop a FGS counterpart. The major advantage of this approach arises from the well-characterized clinical performance of TOC and IR800, which, when combined with analysis of recent FGS clinical trials, provided an experimental strategy that examined key clinical

endpoints such as optimal imaging time points and injection dose, and efficacy for tumor demarcation.

During surgery, differential uptake of a FGS agent in tumor and normal tissues is critical to produce the necessary contrast to identify tumors, margins, residual disease in the wound bed, and regional lymph nodes metastases. One determinant for obtaining maximal contrast is identification of the optimal imaging time point. We previously showed that ^{68}Ga-MMC(IR800)-TOC undergoes time-dependent elimination from circulation and normal tissues up to 3 h post-injection (12) and selected this time point for the initial *in vivo* NIRF imaging studies. Since tumors were not consistently delineated at 3 h, we hypothesized that low agent accumulation, slow clearance from non-target sites, or a combination of the two were contributing factors. Therefore, NIRF imaging was repeated at 24 h and showed improved tumor contrast that was attributed to lower background signal (i.e., washout). Since optical imaging is inherently semi-quantitative (29), we applied the radiolabeling utility of the MMC to produce dual-labeled analogs for early (^{68}Ga) and delayed (^{67}Ga) biodistribution studies that would serve as the gold standard for quantification of tissue uptake. The biodistribution profiles showed that the improved contrast at 24 h was attributable to persistent tumor signal and clearance from background organs. Biodistribution analysis at 48 h supported this observation and produced the highest TBRs. Importantly, the quantitative data obtained by gamma counting were identical to the *ex vivo* optical data and demonstrate the utility of dual-labeling for agent validation.

Image contrast is also dependent upon identifying the optimal injection dose of a FGS agent. Since the final formulation of a radiotracer contains a mixture of unlabeled precursor and the radiolabeled product, administering higher doses could result in competition for binding sites and reduce radioactive signal in tumors. Fluorescent agents, however, generally consist of a single chemical species and do not experience such effects. Thus, FGS agents may benefit from injecting higher doses. This has indeed been shown in a dose escalation study in patients with IR800-conjugated cetuximab where higher TBRs were obtained with the highest injection dose (5), as well as with a fluorescent diabody targeting an anti-prostate stem cell antigen (30). However, numerous studies have reported better TBRs with lower doses since increasing the injection amount also leads to more nontarget uptake that reduces contrast, increases the number of false-positives, and negatively affects specificity (31–34). In order to examine this effect with Ga-MMC(IR800)-TOC, xenografts were injected with 0.5 or 2 nmol and showed a direct correlation between injected dose and absolute fluorescence in tumor and normal tissues. Although the 2 nmol dose produced a nearly 4-fold increase in tumor fluorescence, the TBRs were all higher in the low-dose group. This is likely attributable to non-specific binding of Ga-MMC(IR800)-TOC that is amplified at higher doses. Given the excellent tumor targeting of Ga-MMC(IR800)-TOC and the availability of NIRF imaging systems that can detect microdose levels of dye, further dose optimization studies could identify maximal TBRs that reduce false-positives and enhance diagnostic accuracy.

The efficacy of a FGS agent has been defined by FDA guidance documents as the ability to locate and outline normal structures or distinguish between normal and abnormal anatomy (24). Therefore, efficacy is dependent upon the specificity of the agent for its target and its

overexpression in tumor tissue. We previously showed SSTR2-mediated uptake of ^{64}Cu-MMC(IR800)-TOC *in vitro* and *in vivo*, where competition with octreotide strongly reduced uptake in SSTR2-expressing tumors (35). In a subsequent study with ^{68}Ga-MMC(IR800)-TOC, we demonstrated selective *in vitro* uptake by SSTR2-expressing cells that was 20-fold higher than cells that lacked the receptor, as well as a 16-fold reduction in uptake when co-incubated with octreotide (12). The present study confirms SSTR2-mediated uptake of Ga-MMC(IR800)-TOC *in vivo* as shown by clear differences in tumor fluorescence between HCT116-SSTR2 and HCT116-WT tumors macroscopically (*in vivo*, *ex vivo*) and microscopically.

Non-specific binding of a FGS agent must also be examined as it will affect image contrast in the surgical field-of-view and, thus, efficacy. Surgical resection of primary NETs is most commonly performed in the pancreas, small intestine, or lungs. Therefore, it is imperative that Ga-MMC(IR800)-TOC exhibits low uptake in these tissues in order to generate sufficient contrast for identification of surgical margins or lymph node metastases. Despite endogenous SSTR2 expression in these tissues (94% homology between mouse and human SSTR2 isoforms (36)), *ex vivo* optical imaging in mice at 48 h produced TBRs>4. The highest TBRs were found in the small intestine (17.2±3.5), muscle (15.3±5.0), and lungs (7.6±2.0), suggesting even higher detection sensitivity for sub-clinical disease in these sites. Given the use of numerous drug-device combinations in preclinical and clinical studies, a definitive TBR threshold that indicates a positive fluorescent signal is difficult to define. However, successful intraoperative visualization of tumors has been demonstrated with several targeted agents that produce TBRs>2 (5,37,38) and suggests that contrast ratios for Ga-MMC(IR800)-TOC may be sufficient for tumor identification in a clinical setting.

Intraoperative frozen section analysis is widely used for assessment of margin status and can show the tumor edge by demarcation of tumor from normal tissue by H&E staining. When combined with IHC, this method can identify SSTR2 expression and distribution within tissues and confirm the specificity of Ga-MMC(IR800)-TOC binding. Using frozen sections prepared from mouse xenografts injected with Ga-MMC(IR800)-TOC, we obtained fluorescence images that delineated HCT116-SSTR2 tumors from normal tissue in a manner that was consistent with tumor morphology shown by H&E staining and IHC. HCT116-WT tumors had negative IHC staining and minimal fluorescence. As shown by *ex vivo* tissue imaging, minimal signal was found in normal tissues and shows the potential effectiveness of Ga-MMC(IR800)-TOC for identifying tissues based on overexpression of SSTR2.

Clinically, *ex vivo* macroscopic imaging has emerged as an effective validation method with implications for fluorescence-guided pathology. A recent clinical study used an *ex vivo* fluorescence imaging platform to assess the microdistribution, tumor specificity, and margin identification ability of bevacizumab-IR800 and showed excellent sensitivity and negative predictive value for margin detection (39). The authors also proposed this approach as a first step in the development of novel FGS agents to show tumor-specific binding prior to more specific studies for dose-finding, time point optimization, and assessment of diagnostic accuracy. Similarly, we used Ga-MMC(IR800)-TOC for *ex vivo* staining of fresh biospecimens obtained from patients with pancreatic NETs to examine the ability of our agent to bind to human tumors. In addition to showing intense and preferential uptake in

tumor regions, Ga-MMC(IR800)-TOC staining accurately maintained the tumor boundaries depicted by H&E and may enable margin detection *in situ*. These results compare favorably with *ex vivo* clinical data from several FGS agents (38–40) and could potentially lead to image-based prioritization of margin samples to support current surgical pathology practices. The most impactful application of Ga-MMC(IR800)-TOC, however, may be for real-time surgical imaging. For patients with pancreatic NETs (e.g., gastrinomas, VIPomas, somatostatinomas, and insulinomas), intraoperative tumor localization with Ga-MMC(IR800)-TOC could provide better specificity and stronger NIRF signal than currently used methylene-blue imaging (41,42). Ga-MMC(IR800)-TOC may also enhance the ability of the surgeon to achieve greater debulking of metastatic burden, which can be beneficial both from a symptom management and overall survival standpoint (43). Thus, delineating the tumor with fluorescence might permit more complete cytoreduction, and improve outcomes for patients with metastatic NETs.

In summary, we demonstrated for the first time that an SSTR2-targeted FGS agent can be used for highly specific tumor targeting. Our data showed the effectiveness of radiolabeling in the preclinical characterization of a FGS agent by providing definitive measurements of agent biodistribution that support imaging data. Imaging at the macro, meso, and microscopic levels, provided extensive validation of SSTR2 specificity, which were extended to human NETs and indicate significant promise for *in vivo* application of Ga-MMC(IR800)-TOC. Our approach can be used in combination with SSTR2-targeted radiotracers (i.e., ^{68}Ga-DOTA-TOC and ^{68}Ga-DOTA-TATE) to identify patients that are candidates for FGS, thereby improving surgical care for patients with NETs.

Supplementary Material

Refer to Web version on PubMed Central for supplementary material.

Acknowledgements

This work was supported by the National Institute of Biomedical Imaging and Bioengineering (R01 EB017279), National Cancer Institute (P30 CA008748, K99 CA218875–01A1), the Tow Foundation, and Memorial Sloan Kettering Cancer Center's Center for Molecular Imaging & Nanotechnology. The authors thank Martina Cagigas and Amy McElhany for assistance with surgical biospecimens, and Dr. Erik Wilson and Armando Garcia for access to the Memorial Hermann Surgical Innovation and Robotics Institute. The authors also acknowledge the support of the Imaging Core Facility at The University of Texas Health Science Center-Center for Molecular Imaging, and the Radiochemistry & Molecular Imaging Probes Core Facility and Molecular Cytology Core Facility at Memorial Sloan Kettering Cancer Center.

References

1. Yao JC, Lagunes DR, Kulke MH. Targeted therapies in neuroendocrine tumors (NET): clinical trial challenges and lessons learned. The oncologist 2013;18(5):525–32 doi 10.1634/theoncologist.2012-0434. [PubMed: 23615698]
2. Maggard MA, O'Connell JB, Ko CY. Updated population-based review of carcinoid tumors. Annals of surgery 2004;240(1):117–22. [PubMed: 15213627]
3. Birnbaum DJ, Turrini O, Vigano L, Russolillo N, Autret A, Moutardier V, et al. Surgical management of advanced pancreatic neuroendocrine tumors: short-term and long-term results from an international multi-institutional study. Annals of surgical oncology 2015;22(3):1000–7 doi 10.1245/s10434-014-4016-8. [PubMed: 25190116]

4. Mayo SC, de Jong MC, Pulitano C, Clary BM, Reddy SK, Gamblin TC, et al. Surgical Management of Hepatic Neuroendocrine Tumor Metastasis: Results from an International Multi-Institutional Analysis. Annals of Surgical Oncology 2010;17(12):3129–36 doi 10.1245/s10434-010-1154-5. [PubMed: 20585879]
5. Rosenthal EL, Warram JM, de Boer E, Chung TK, Korb ML, Brandwein-Gensler M, et al. Safety and Tumor Specificity of Cetuximab-IRDye800 for Surgical Navigation in Head and Neck Cancer. Clinical cancer research : an official journal of the American Association for Cancer Research 2015;21(16):3658–66 doi 10.1158/1078-0432.CCR-14-3284. [PubMed: 25904751]
6. Reubi JC, Schonbrunn A. Illuminating somatostatin analog action at neuroendocrine tumor receptors. Trends in pharmacological sciences 2013;34(12):676–88 doi 10.1016/j.tips.2013.10.001. [PubMed: 24183675]
7. Rodrigues M, Traub-Weidinger T, Li S, Ibi B, Virgolini I. Comparison of ^{111}In-DOTA-DPhe1-Tyr3-octreotide and ^{111}In-DOTA-lanreotide scintigraphy and dosimetry in patients with neuroendocrine tumours. European journal of nuclear medicine and molecular imaging 2006;33(5):532–40 doi 10.1007/s00259-005-0020-3. [PubMed: 16491425]
8. Gabriel M, Muehllechner P, Decristoforo C, von Guggenberg E, Kendler D, Prommegger R, et al. 99mTc-EDDA/HYNIC-Tyr(3)-octreotide for staging and follow-up of patients with neuroendocrine gastro-entero-pancreatic tumors. The quarterly journal of nuclear medicine and molecular imaging : official publication of the Italian Association of Nuclear Medicine 2005;49(3):237–44.
9. Win Z, Al-Nahhas A, Towey D, Todd JF, Rubello D, Lewington V, et al. ^{68}Ga-DOTATATE PET in neuroectodermal tumours: first experience. Nuclear medicine communications 2007;28(5):359–63 doi 10.1097/MNM.0b013e32808ea0b0. [PubMed: 17414885]
10. Hofmann M, Maecke H, Borner R, Weckesser E, Schoffski P, Oei L, et al. Biokinetics and imaging with the somatostatin receptor PET radioligand (68)Ga-DOTATOC: preliminary data. Eur J Nucl Med 2001;28(12):1751–7 doi 10.1007/s002590100639. [PubMed: 11734911]
11. Wild D, Macke HR, Waser B, Reubi JC, Ginj M, Rasch H, et al. 68Ga-DOTANOC: a first compound for PET imaging with high affinity for somatostatin receptor subtypes 2 and 5. European journal of nuclear medicine and molecular imaging 2005;32(6):724 doi 10.1007/s00259-004-1697-4. [PubMed: 15551131]
12. Ghosh SC, Hernandez Vargas S, Rodriguez M, Kossatz S, Voss J, Carmon KS, et al. Synthesis of a Fluorescently Labeled (68)Ga-DOTA-TOC Analog for Somatostatin Receptor Targeting. ACS medicinal chemistry letters 2017;8(7):720–5 doi 10.1021/acsmedchemlett.7b00125. [PubMed: 28740605]
13. Hall MA, Kwon S, Robinson H, Lachance PA, Azhdarinia A, Ranganathan R, et al. Imaging prostate cancer lymph node metastases with a multimodality contrast agent. The Prostate 2012;72(2):129–46 doi 10.1002/pros.21413. [PubMed: 21538422]
14. Zhang H, Moroz MA, Serganova I, Ku T, Huang R, Vider J, et al. Imaging expression of the human somatostatin receptor subtype-2 reporter gene with 68Ga-DOTATOC. Journal of nuclear medicine : official publication, Society of Nuclear Medicine 2011;52(1):123–31 doi 10.2967/jnumed.110.079004.
15. Sun L, Luo J, Mackey LV, Morris LM, Franko-Tobin LG, LePage KT, et al. Investigation of cancer cell lines for peptide receptor-targeted drug development. J Drug Target 2011;19(8):719–30 doi 10.3109/1061186X.2011.558089. [PubMed: 21830941]
16. Schmitt A, Bernhardt P, Nilsson O, Ahlman H, Kolby L, Forssell-Aronsson E. Differences in biodistribution between 99mTc-depreotide, 111In-DTPA-octreotide, and 177Lu-DOTA-Tyr3-octreotate in a small cell lung cancer animal model. Cancer Biother Radiopharm 2005;20(2):231–6 doi 10.1089/cbr.2005.20.231. [PubMed: 15869461]
17. Hosono M, Hosono MN, Haberberger T, Zamora PO, Guhlke S, Bender H, et al. Localization of small-cell lung cancer xenografts with iodine-125-, indium-111-, and rhenium-188-somatostatin analogs. Jpn J Cancer Res 1996;87(9):995–1000. [PubMed: 8878464]
18. Lewin J, Cullinane C, Akhurst T, Waldeck K, Watkins DN, Rao A, et al. Peptide receptor chemoradionuclide therapy in small cell carcinoma: from bench to bedside. European journal of nuclear medicine and molecular imaging 2015;42(1):25–32 doi 10.1007/s00259-014-2888-2. [PubMed: 25125202]

19. Santini C, Kuil J, Bunschoten A, Pool S, de Blois E, Ridwan Y, et al. Evaluation of a Fluorescent and Radiolabeled Hybrid Somatostatin Analog In Vitro and in Mice Bearing H69 Neuroendocrine Xenografts. Journal of nuclear medicine : official publication, Society of Nuclear Medicine 2016;57(8):1289–95 doi 10.2967/jnumed.115.164970.
20. Nayak TK, Atcher RW, Prossnitz ER, Norenberg JP. Enhancement of somatostatin-receptor-targeted (177)Lu-[DOTA(0)-Tyr(3)]-octreotide therapy by gemcitabine pretreatment-mediated receptor uptake, up-regulation and cell cycle modulation. Nucl Med Biol 2008;35(6):673–8 doi 10.1016/j.nucmedbio.2008.05.003. [PubMed: 18678352]
21. van Dam GM, Themelis G, Crane LM, Harlaar NJ, Pleijhuis RG, Kelder W, et al. Intraoperative tumor-specific fluorescence imaging in ovarian cancer by folate receptor-alpha targeting: first in-human results. Nature medicine 2011;17(10):1315–9 doi 10.1038/nm.2472.
22. Nagaya T, Nakamura YA, Choyke PL, Kobayashi H. Fluorescence-Guided Surgery. Frontiers in oncology 2017;7:314 doi 10.3389/fonc.2017.00314. [PubMed: 29312886]
23. Tummers WS, Warram JM, Tipirneni KE, Fengler J, Jacobs P, Shankar L, et al. Regulatory Aspects of Optical Methods and Exogenous Targets for Cancer Detection. Cancer research 2017;77(9): 2197–206 doi 10.1158/0008-5472.CAN-16-3217. [PubMed: 28428283]
24. Rosenthal EL, Warram JM, de Boer E, Basilion JP, Biel MA, Bogyo M, et al. Successful Translation of Fluorescence Navigation During Oncologic Surgery: A Consensus Report. Journal of nuclear medicine : official publication, Society of Nuclear Medicine 2016;57(1):144–50 doi 10.2967/jnumed.115.158915.
25. Kaemmerer D, Prasad V, Daffner W, Haugvik SP, Senftleben S, Baum RP, et al. Radioguided surgery in neuroendocrine tumors using Ga-68-labeled somatostatin analogs: a pilot study. Clinical nuclear medicine 2012;37(2):142–7 doi 10.1097/RLU.0b013e3182291de8. [PubMed: 22228336]
26. Sadowski SM, Millo C, Neychev V, Aufforth R, Keutgen X, Glanville J, et al. Feasibility of Radio-Guided Surgery with (6)(8)Gallium-DOTATATE in Patients with Gastro-Entero-Pancreatic Neuroendocrine Tumors. Annals of surgical oncology 2015;22 Suppl 3:S676–82 doi 10.1245/s10434-015-4857-9. [PubMed: 26350374]
27. Kuil J, Velders AH, van Leeuwen FW. Multimodal tumor-targeting peptides functionalized with both a radio- and a fluorescent label. Bioconjugate chemistry 2010;21(10):1709–19 doi 10.1021/bc100276j. [PubMed: 20812730]
28. Azhdarinia A, Ghosh P, Ghosh S, Wilganowski N, Sevick-Muraca EM. Dual-labeling strategies for nuclear and fluorescence molecular imaging: a review and analysis. Molecular imaging and biology : MIB : the official publication of the Academy of Molecular Imaging 2012;14(3):261–76 doi 10.1007/s11307-011-0528-9. [PubMed: 22160875]
29. Zhang RR, Schroeder AB, Grudzinski JJ, Rosenthal EL, Warram JM, Pinchuk AN, et al. Beyond the margins: real-time detection of cancer using targeted fluorophores. Nature reviews Clinical oncology 2017;14(6):347–64 doi 10.1038/nrclinonc.2016.212.
30. Sonn GA, Behesnilian AS, Jiang ZK, Zettlitz KA, Lepin EJ, Bentolila LA, et al. Fluorescent Image-Guided Surgery with an Anti-Prostate Stem Cell Antigen (PSCA) Diabody Enables Targeted Resection of Mouse Prostate Cancer Xenografts in Real Time. Clinical cancer research : an official journal of the American Association for Cancer Research 2016;22(6):1403–12 doi 10.1158/1078-0432.CCR-15-0503. [PubMed: 26490315]
31. Tummers WS, Miller SE, Teraphongphom NT, Gomez A, Steinberg I, Huland DM, et al. Intraoperative Pancreatic Cancer Detection using Tumor-Specific Multimodality Molecular Imaging. Annals of surgical oncology 2018;25(7):1880–8 doi 10.1245/s10434-018-6453-2. [PubMed: 29667116]
32. Hoogstins CE, Tummers QR, Gaarenstroom KN, de Kroon CD, Trimbos JB, Bosse T, et al. A Novel Tumor-Specific Agent for Intraoperative Near-Infrared Fluorescence Imaging: A Translational Study in Healthy Volunteers and Patients with Ovarian Cancer. Clinical cancer research : an official journal of the American Association for Cancer Research 2016;22(12):2929–38 doi 10.1158/1078-0432.CCR-15-2640. [PubMed: 27306792]
33. Mahalingam SM, Dudkin VY, Goldberg S, Klein D, Yi F, Singhal S, et al. Evaluation of a Centyrin-Based Near-Infrared Probe for Fluorescence-Guided Surgery of Epidermal Growth Factor Receptor Positive Tumors. Bioconjugate chemistry 2017;28(11):2865–73 doi 10.1021/acs.bioconjchem.7b00566. [PubMed: 28945346]

34. Rosenthal EL, Moore LS, Tipirneni K, de Boer E, Stevens TM, Hartman YE, et al. Sensitivity and Specificity of Cetuximab-IRDye800CW to Identify Regional Metastatic Disease in Head and Neck Cancer. Clinical cancer research : an official journal of the American Association for Cancer Research 2017;23(16):4744–52 doi 10.1158/1078-0432.CCR-16-2968. [PubMed: 28446503]

35. Ghosh SC, Rodriguez M, Carmon KS, Voss J, Wilganowski NL, Schonbrunn A, et al. A Modular Dual-Labeling Scaffold That Retains Agonistic Properties for Somatostatin Receptor Targeting. Journal of nuclear medicine : official publication, Society of Nuclear Medicine 2017;58(11):1858–64 doi 10.2967/jnumed.116.187971.

36. Reisine T, Bell GI. Molecular biology of somatostatin receptors. Endocr Rev 1995;16(4):427–42 doi 10.1210/edrv-16-4-427. [PubMed: 8521788]

37. Predina JD, Newton AD, Keating J, Dunbar A, Connolly C, Baldassari M, et al. A Phase I Clinical Trial of Targeted Intraoperative Molecular Imaging for Pulmonary Adenocarcinomas. The Annals of thoracic surgery 2018;105(3):901–8 doi 10.1016/j.athoracsur.2017.08.062. [PubMed: 29397932]

38. Gao RW, Teraphongphom NT, van den Berg NS, Martin BA, Oberhelman NJ, Divi V, et al. Determination of Tumor Margins with Surgical Specimen Mapping Using Near-Infrared Fluorescence. Cancer research 2018 doi 10.1158/0008-5472.CAN-18-0878.

39. Lamberts LE, Koch M, de Jong JS, Adams ALL, Glatz J, Kranendonk MEG, et al. Tumor-Specific Uptake of Fluorescent Bevacizumab-IRDye800CW Microdosing in Patients with Primary Breast Cancer: A Phase I Feasibility Study. Clinical cancer research : an official journal of the American Association for Cancer Research 2017;23(11):2730–41 doi 10.1158/1078-0432.CCR-16-0437. [PubMed: 28119364]

40. Predina JD, Newton AD, Corbett C, Xia L, Shin M, Sulfyok LF, et al. A Clinical Trial of TumorGlow(R) to Identify Residual Disease during Pleurectomy and Decortication. The Annals of thoracic surgery 2018 doi 10.1016/j.athoracsur.2018.06.015.

41. Handgraaf HJM, Boogerd LSF, Shahbazi Feshtali S, Farina Sarasqueta A, Snel M, Swijnenburg RJ, et al. Intraoperative Near-Infrared Fluorescence Imaging of Multiple Pancreatic Neuroendocrine Tumors: A Case Report. Pancreas 2018;47(1):130–3 doi 10.1097/MPA.0000000000000951. [PubMed: 29232342]

42. Winer JH, Choi HS, Gibbs-Strauss SL, Ashitate Y, Colson YL, Frangioni JV. Intraoperative localization of insulinoma and normal pancreas using invisible near-infrared fluorescent light. Annals of surgical oncology 2010;17(4):1094–100 doi 10.1245/s10434-009-0868-8. [PubMed: 20033320]

43. Morgan RE, Pommier SJ, Pommier RF. Expanded criteria for debulking of liver metastasis also apply to pancreatic neuroendocrine tumors. Surgery 2018;163(1):218–25 doi 10.1016/j.surg.2017.05.030. [PubMed: 29103583]

Statement of translational relevance

Surgery plays a prominent role in the treatment of neuroendocrine tumors (NETs) and can be curative if all tumors are detected and removed. Currently, there are no targeted fluorescent intraoperative imaging agents clinically available to assist surgeons in identifying NETs in real-time and, thus, these patients experience remarkably high cancer recurrence rates. Radiolabeled somatostatin analogs, such as ^{68}Ga-DOTA-TOC, are excellent models for the development of fluorescent analogs based on their high diagnostic accuracy for detecting somatostatin receptor subtype-2 (SSTR2) expressing tumors in patients. Here, we report the *in vivo* and *ex vivo* tumor imaging with the multimodality agent, Ga-MMC(IR800)-TOC, and provide the first evidence that a somatostatin analog may have potential utility for fluorescence-guided surgery (FGS). Translational endpoints for an FGS agent, such as identification of optimal imaging time point, dose optimization, and demonstration of efficacy, are examined to show the potential of the agent for clinical use.

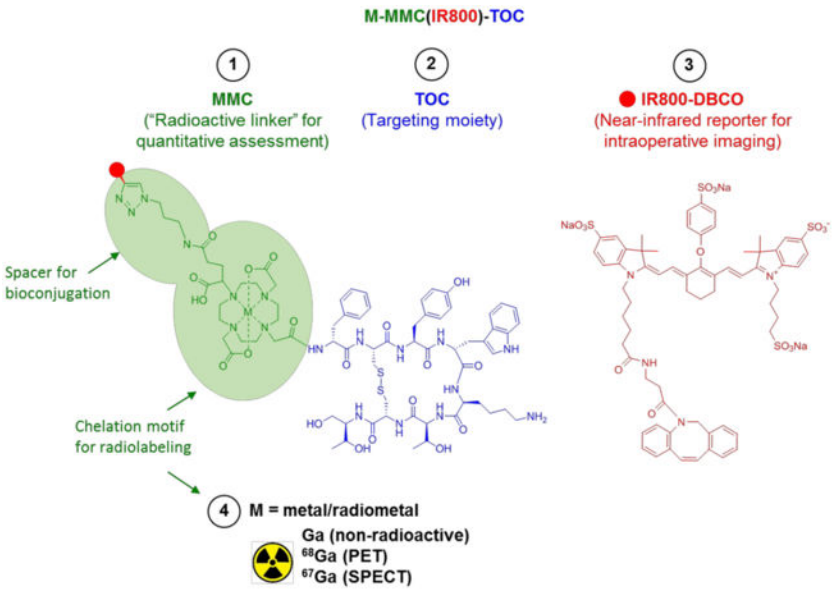

Figure 1. Structure and components of the SSTR2-targeted intraoperative imaging agent.
MMC-mediated radiolabeling enables quantitative characterization of the fluorescent somatostatin analog, MMC(IR800)-TOC.

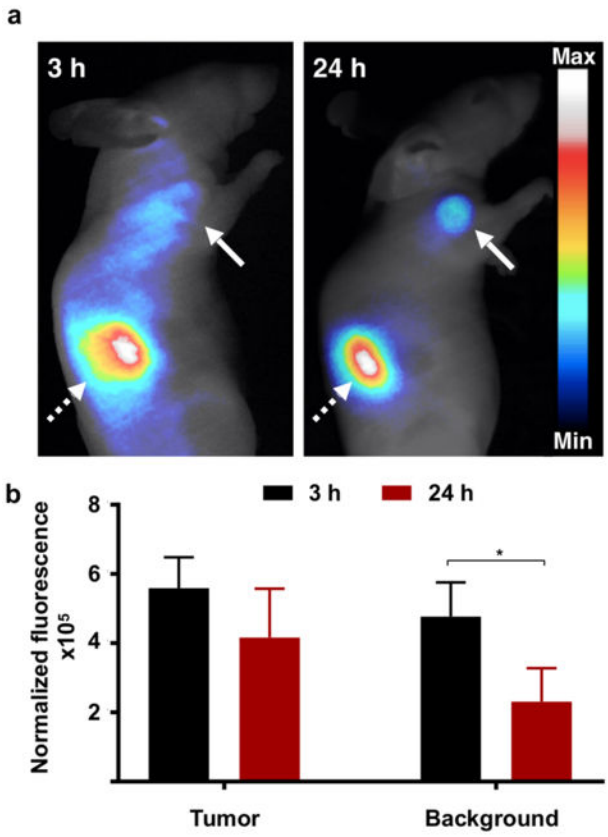

Figure 2. ***In vivo*** **NIRF imaging of Ga-MMC(IR800)-TOC in mice.**

(a) Representative NIRF images of Ga-MMC(IR800)-TOC were acquired in HCT116-SSTR2 xenografts at early and delayed time points using an EMCCD fluorescence imaging system. Solid arrows indicate tumor, dashed arrows indicate kidney. Background measurements were obtained near the hind limb. (b) Normalized fluorescence signal (displayed as counts/pixel^2) in tumor and background tissue. *$P < 0.005$.

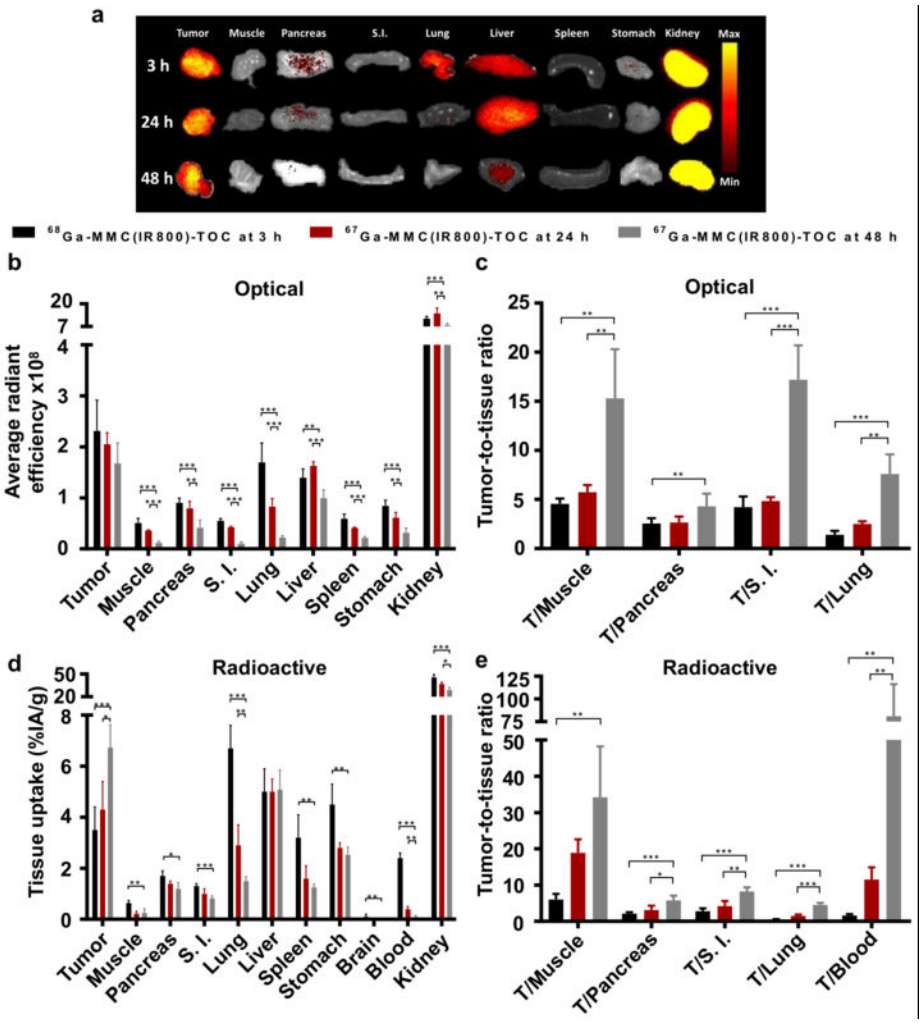

Figure 3. Qualitative and quantitative assessment of biodistribution.

(a) *Ex vivo* optical images (IVIS) of organs resected from HCT116-SSTR2 xenografts that were injected with ^{68}Ga-MMC(IR800)-TOC (3 h) or ^{67}Ga-MMC(IR800)-TOC (24 and 48 h). Determination of (b) tissue fluorescence by analysis of NIRF images and (c) corresponding contrast ratios at major sites of NET incidence (pancreas, small intestine, lung) and selected non-target sites (muscle and blood). Determination of (d) radioactive uptake by gamma counting and (e) corresponding TBRs. $*P < 0.05$, $**P < 0.01$, $***P < 0.001$. Data are presented as mean ± standard deviation (n=5). Average radiant efficiency displayed as ([p/s/cm^2/sr]/[μW/cm^2]). S.I., small intestine.

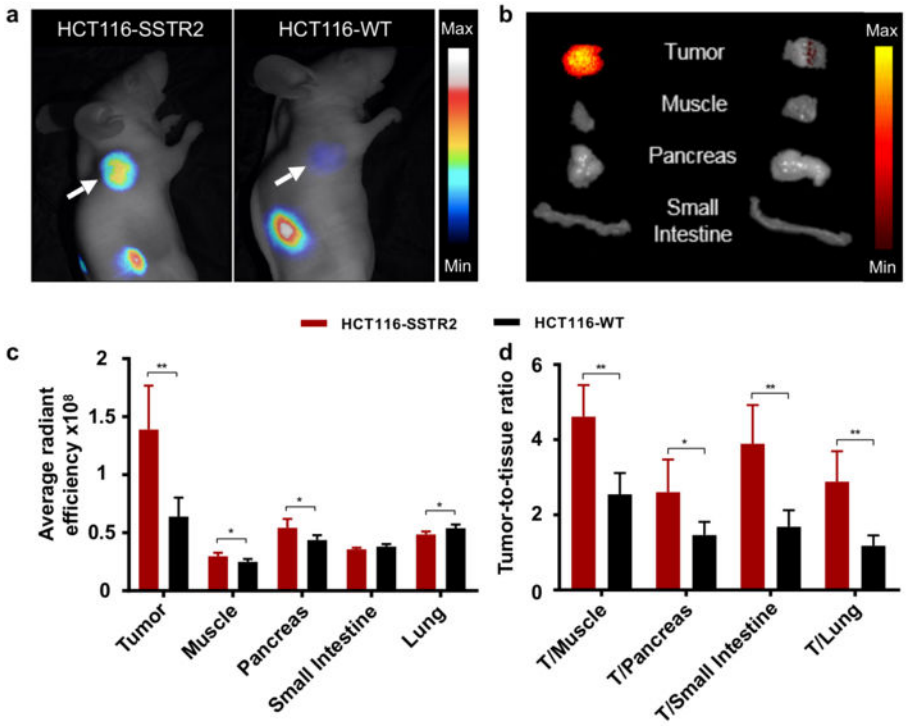

Figure 4. *In vivo* and *ex vivo* specificity of Ga-MMC(IR800)-TOC.

(a) *In vivo* NIRF imaging in HCT116-SSTR2 and HCT116-WT subcutaneous xenografts acquired 24 h post-injection (EMCCD), arrows indicate tumor. (b) *Ex vivo* NIRF imaging of selected organs (IVIS) and (c) tissue fluorescence determined from image analysis. (d) Optical contrast provided by the ratio of the average fluorescent signal in the tumor to sites of NET formation. $*P < 0.05$, $**P < 0.01$, $***P < 0.001$. Data are presented as mean ± standard deviation (n=5). Average radiant efficiency displayed as ([p/s/cm^2/sr]/[μW/cm^2]).

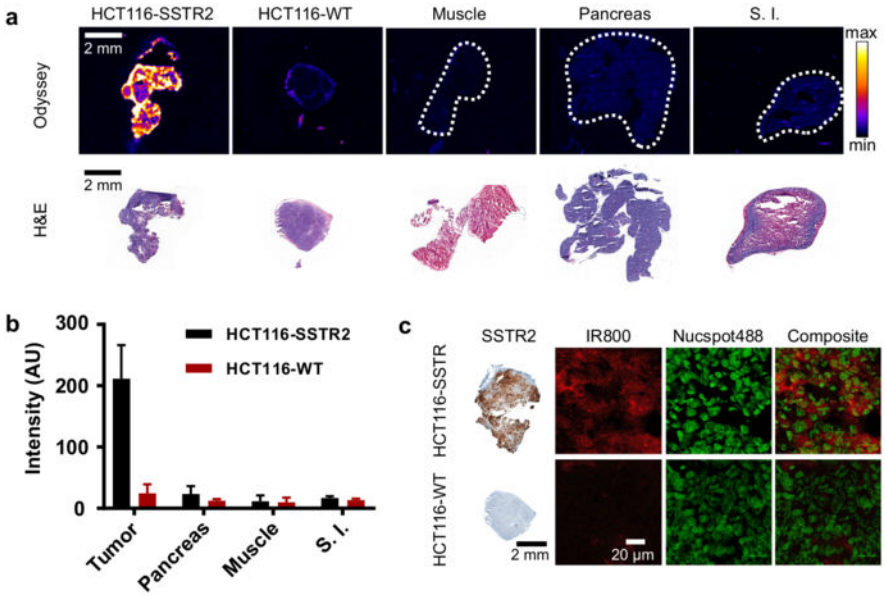

Figure 5. Multiscale imaging of Ga-MMC(IR800)-TOC uptake.

(a) Confirmation of *in vivo* accumulation of Ga-MMC(IR800)-TOC in HCT116-SSTR2 and HCT116-WT xenografts and organs *via* NIRF imaging of frozen sections. (b) Quantification of the fluorescence signal of tumor and frozen section scans (Data are presented as mean ± standard deviation n=3 animals/group). (c) Microscopic detection of *in vivo* injected Ga-MMC(IR800)-TOC. Frozen sections from resected HCT116-SSTR2 and HCT116-WT tumors were counterstained with a nuclear stain (Nucspot488), fixed, and examined by confocal microscopy. S.I., small intestine.

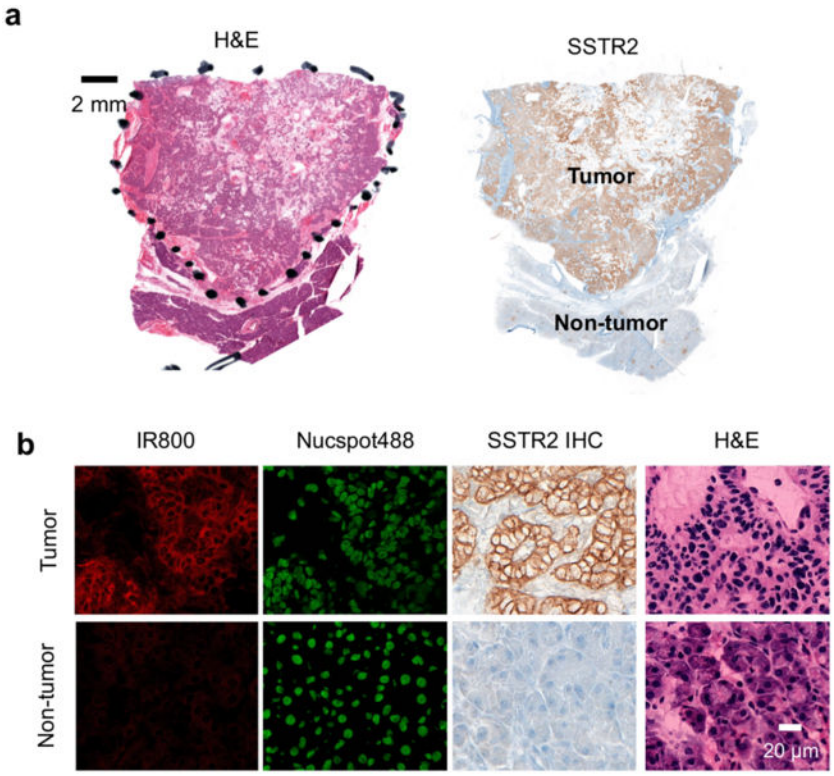

Figure 6. Ga-MMC(IR800)-TOC binding in human NET biospecimens.

(a) H&E and SSTR2 IHC staining of frozen sections prepared from a surgically resected human pancreatic NET. (b) *Ex vivo* staining of an unfixed frozen section from the same tumor with Ga-MMC(IR800)-TOC. Nuclei were counterstained with Nucspot488. H&E staining was conducted for morphological reference.